Nanoscale

Dynamic Article Links

Cite this: *Nanoscale*, 2012, **4**, 3135

www.rsc.org/nanoscale

PAPER

Facile synthesis of fluorescent porous zinc sulfide nanospheres and their application for potential drug delivery and live cell imaging†

Ruimin Xing and Shanhu Liu*

Received 27th November 2011, Accepted 12th March 2012
DOI: 10.1039/c2nr11860b

Fabrication of intrinsically fluorescent porous nanocarriers that are simultaneously stable in aqueous solutions and photostable is critical for their application in drug delivery and optical imaging but remains a challenge. In this study, fluorescent porous zinc sulfide nanospheres were synthesized by a facile gum arabic-assisted hydrothermal procedure. The morphology, composition and properties of the nanospheres have been characterized by field-emission scanning electron microscopy, transmission electron microscopy, X-ray powder diffraction, N_2 adsorption-desorption analysis, thermal gravimetric analysis, fourier transform infrared spectrograph, optical measurement, dynamic light scattering, and cytotoxicity assay. They exhibit larger surface area, excellent colloidal stability, photostable fluorescent signals, and good biocompatibility, which makes them promising hosts for drug delivery and cellular imaging. The fluorescent dye safranine-T was employed as a drug model and loaded into the porous nanospheres, which were delivered to human cervical cancer HeLa cells *in vitro* for live cell imaging.

1. Introduction

Drug delivery systems (DDSs) that are being developed to improve the therapeutic index of small molecule drugs have attracted increasing attention in recent years.[1,2] They are mainly composed of particulate carriers and clinical drugs. Therefore, the fabrication of proper carriers is the foremost step to achieve a desirable delivery.[3–5] Among them, multifunctional nanoparticles that are simultaneously porous and fluorescent have evoked intensive interest because they can function as carriers for substantial loading and delivery of drugs while being tracked by fluorescence imaging in real time.[6–9]

However, current carriers are usually made of porous nanomaterials (*e.g.* mesoporous silica, porous magnetic and carbon nanoparticles) modified with fluorescent substances (*e.g.* organic dyes, fluorescent proteins and semiconductor quantum dots).[9–13] These modified DDSs might have some drawbacks: (a) tedious synthetic procedures for the porous materials and for the fluorescent decoration; (b) their properties may vary from batch to batch; once introduced, the modification may interfere with the very processes they are meant to monitor;[14] (c) cadmium-based QDs are likely to partially decompose and release highly toxic Cd^{2+} ions, which are fatal to living cells.[15,16] Therefore, a facile route is highly desirable to fabricate a kind of intrinsically fluorescent porous nanocarriers for drug delivery and optical imaging. Recently, intrinsically luminescent porous silicon nanoparticles and Eu-doped amorphous calcium phosphate porous nanospheres were fabricated to cater for this intention.[17,18]

In some respects, fluorescent zinc sulfide semiconductors are a powerful alternative to organic dyes and cadmium-based QDs in terms of their non-toxicity and stability against degradation.[19] For example, several composites such as Mn:ZnSe/ZnS QDs and Fe_3O_4/ZnS hollow nanospheres have been explored and the incorporation of ZnS was found to improve the biocompatible and photostable fluorescent properties.[20,21] However, ZnS semiconductors, and especially porous nanostructures, remain relatively under-explored in terms of delivery systems and live cell imaging.

In this work, intrinsically fluorescent porous zinc sulfide nanospheres (ZnS FPNSs) are synthesized by a facile gum arabic-assisted hydrothermal procedure. ZnS FPNSs offer photostable fluorescent signals and possess excellent colloidal stability and biocompatible features. Their porous structure gives them promise as a drug delivery carrier and allows substantial loading and sustained release of drugs. The fluorescent dye safranine-T (ST) was employed as a drug model and loaded into ZnS FPNSs, which were delivered to human cervical cancer HeLa cells *in vitro* for live cell imaging.

2. Experimental

2.1 Materials

Gum Arabic (GA) was purchased from Sigma–Aldrich. $ZnAc_2 \cdot 2H_2O$, thioacetamide (TAA) and other chemical reagents

Institute of Molecular and Crystal Engineering, College of Chemistry and Chemical Engineering, Henan University, Kaifeng, P.R. China. E-mail: shanhuliu@henu.edu.cn; Tel: +86 378-3881589

† Electronic supplementary information (ESI) available. See DOI: 10.1039/c2nr11860b

were obtained from Nanjing Chemical Reagent Co., Ltd. All chemicals were directly used as received without further purification. Millipore water (18.2 MΩ cm at 25 °C) was used throughout all of the experiments.

2.2 Preparation of ZnS FPNSs

ZnS FPNSs were synthesized in one pot *via* a hydrothermal route. In a typical procedure, $ZnAc_2 \cdot 2H_2O$ (1 mmol), GA (0.1 g) and TAA (1 mmol) were dissolved in water (20 mL) in the order stated and ultrasonicated vigorously to obtain a clear solution. The mixed solution was transferred into a Teflon-line autoclave and maintained at 120 °C for 12 h. The white solid products were collected by centrifugation and washed at least three times with water and ethanol. They were then dried at 50 °C before characterization and application.

2.3 Loading ST inside ZnS FPNSs and its release properties

ST was loaded into ZnS FPNSs by mixing 90 mg of the nanospheres with 30 mL of an aqueous solution of ST (3 mg mL^{-1}) overnight in the dark at room temperature. The resulting suspension was centrifuged at 9000 rpm for 20 min, washed with water several times and then dried at 50 °C overnight. The amount of ST loaded into the nanospheres was estimated by comparing the fluorescence intensity of the ST solutions before and after loading with a standard curve.[22] The ST-loaded nanospheres are denoted as the ST–ZnS system. The *in vitro* release was carried out in a phosphate buffered saline (PBS, 0.1 M, pH 7.4) solution. Sixty milligrams of the ST–ZnS system were suspended into dialysis bags (MWCO 14 kDa) containing 4 mL of PBS solution, and subsequently dialyzed against 26 mL of PBS solution with constant stirring (~100 rpm) at 37 °C. The release process was monitored by taking an aliquot (2 mL) of the dialysis media at given time intervals by measuring the fluorescence intensity at the wavelength of 578 nm. An aliquot (2 mL) of fresh PBS solution was added to continue the dialysis.

2.4 Cytotoxicity assay

The cytotoxicity of ZnS FPNSs was tested by the 3-(4,5-dimethylthiazol-2-yl)-2,5-diphenyltetrazolium bromide (MTT) assay.[23] HeLa cells were cultured in Dulbecco's Modified Eagle Medium (DMEM, Gibco) supplemented with 10% fetal bovine serum (FBS), penicillin (100 units ml^{-1}), streptomycin (100 mg ml^{-1}) and 5% CO_2 at 37 °C. The cells (*ca.* 5000) were seeded in each well of 96-well plates and incubated overnight. The cells were then treated in triplicate with fresh medium containing grade concentrations of ZnS FPNSs and incubated at 37 °C for 24 h. Untreated cells were used as references. An aliquot of MTT solution (10 μL) was added to each well and the cells incubated for a further 4 h. DMSO (150 μL) was added to each well after the medium was removed, and the absorbance of the purple formazan was recorded at 570 nm using an ELISA plate reader. The cytotoxicity results were calculated based on the data of three replicate tests.

2.5 Live cell imaging

HeLa cells seeded on coverslips were cultured in DMEM medium. After removing the incubation media and rinsing three times with 1 × PBS, the cells were incubated in fresh medium containing the ST–ZnS system for 6 h at 37 °C. Then the cells was washed three times with 1xPBS and imaged using the dual-channel mode of a confocal laser scanning microscope (CLSM) by Zeiss LSM710.

2.6 Characterization

Field emission scanning electron microscopy (FE-SEM) images were obtained using a Hitachi S-4800 field emission electron microscope at an accelerating voltage of 5 kV. Transmission electron microscopy (TEM) images and selected area electron diffraction (SAED) patterns were taken using a JEOL JEM-2100 transmission electron microscope at an accelerating voltage of 200 kV. X-Ray powder diffraction (XRD) measurements were performed on a Japan Shimadzu XRD-6000 diffractometer with Cu-Kα radiation (λ = 0.15418 nm); a scanning rate of 0.05 deg s^{-1} was applied to record the patterns in the 2θ range of 10–80°. N_2 adsorption–desorption isotherms were obtained at 77 K on an ASAP 2020 volumetric adsorption equipment made by Micromeritics Instrument Corporation. The sample was pretreated for 12 h at 373 K under nitrogen before the measurements. Thermal gravimetric analysis (TGA) was performed on a Pyris 1 DTA instrument with a heating rate of 10 °C min^{-1} in a nitrogen flow of 20 mL min^{-1}. Derivative thermogravimetry (DTG) was deduced from the first derivative of the TGA curve. Fourier transform infrared (FT-IR) spectra were recorded on a Nicolet 6700 Fourier transform infrared spectrograph in the range of 4000–500 cm^{-1}. UV–vis absorption and photoluminescence (PL) spectra were performed on a Hitachi U-4100 and F-7000 fluorescence spectrophotometer, respectively. Zeta potentials were measured on a Malven Nano-Z instrument. Hydrodynamic diameters were determined using a BI-200SM dynamic light scattering device (DLS, Brookhaven Instruments Co., Holtsville, NY).

3. Results and discussion

3.1 Preparation and characterization of ZnS FPNSs

ZnS FPNSs were conveniently synthesized by a GA-assisted hydrothermal procedure. Zinc acetate dihydrate was used as zinc source and TAA served as precipitant for slowly releasing sulfide ions. GA was selected because it is a nontoxic, hydrophilic, and highly branched complex of polysaccharides and glycoproteins with abundant hydroxyl and carboxyl groups and has recently been used to stabilize and functionalize several nanoparticles.[24,25] By fine-tuning various reaction conditions such as the concentrations, the reaction temperature and time, these fluorescent porous nanospheres were successfully synthesized.

The morphology and size distribution of ZnS FPNSs were investigated using SEM. As Fig. 1A shows, the product presents a well-defined and uniform spherical morphology with a monodisperse population in large domains. Statistical analysis indicates that the particles have a relatively narrow distribution, with an average diameter of about 70 nm (ESI,† Fig. S1). The XRD

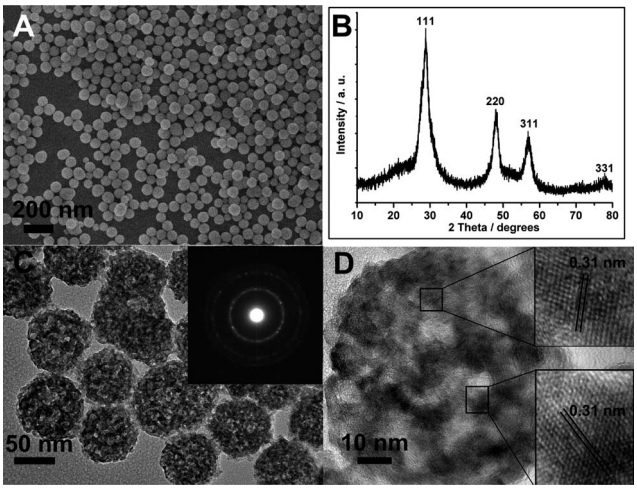

Fig. 1 Typical SEM image (A) and XRD patterns (B) of ZnS FPNSs. Typical low- (C) and high-resolution TEM images (D) of ZnS FPNSs. The inset of C is the SAED pattern of an isolated nanosphere.

patterns in Fig. 1B match well with the standard pattern of cubic zinc blend structure of ZnS (JCPDS file No. 80-0020), with three reflections being Miller indexed as (111), (220), and (311), respectively. Calculations using the Debye–Scherrer formula for the strongest peak (111) showed grain sizes of 5 nm. This result indicates that the nanospheres of 70 nm in size might be made up of small primary particles.

Detailed structural information was obtained by TEM. Shown in Fig. 1C, the distinct contrast within the nanospheres was derived from the difference in electron density, indicating that the nanospheres exhibit a porous structure. The SAED pattern (Inset of Fig. 1C) obtained from an isolated nanosphere shows characteristic diffuse electron diffraction rings, indicative of the polycrystaline-like diffraction profiles. More evidence on its structure and crystallinity was obtained from high-resolution TEM analysis (Fig. 1D). The porous structure is clearly observed, and was assembled by small primary particles with a diameter of about 4 nm, which is in good agreement with the XRD result. The primary particles display high crystallinity with clear lattice fringes. The experimental lattice spacing of 0.31 nm is analogous to the (111) plane of cubic ZnS.

N_2 absorption and desorption analysis was used to further examine the porous structure and the data are shown in Fig. 2. The isotherms feature the type IV curves with a hysteresis loop generated by capillary condensation, which is typical of mesoporous materials.[26] As shown in the inset of Fig. 2, the average pore diameter of the nanospheres is about 6 nm; the sharp distribution around 100 nm suggests that these nanospheres have high monodispersity.[27] The specific surface area and pore volume were determined to be about 132 $m^2\ g^{-1}$ and 0.4 $cm^3\ g^{-1}$, respectively. The relatively large surface area and pore volume strongly support the fact that the nanospheres have a porous structure, which is attractive for loading drugs and the following sustained release.[28]

The thermal stability of ZnS FPNSs was investigated by TGA. The thermograms of GA and ZnS FPNSs are shown in Fig. 3. In the tested temperature range (30–600 °C), GA loses *ca.* 75% weight whereas ZnS FPNSs lose only *ca.* 16% weight. In addition, DTG was used for observing slight changes in weight that are not readily noticed on the TGA curves. As the dashed lines in Fig. 3 show, GA presents a minor peak at 60 °C and a sharp peak at 300 °C on its DTG plot. The weight loss at 60 °C was presumably associated with loss of water corresponding to the moisture content of GA (12%) and the loss at 300 °C was probably due to the combustion and escape of small molecules resulting from the disintegration of GA (63%).[29] In contrast, ZnS FPNSs display a relatively flat DTG plot with two small peaks at 60 °C and 300 °C. The consistency of the inflection point at 300 °C on their DTG plots of GA and ZnS FPNSs suggests that the porous nanospheres contain a GA component with weight percent accounting for *ca.* 20% of the nanospheres.

The involvement of GA or its fragments in ZnS FPNSs was further studied by FT-IR spectroscopy (ESI,† Fig. S2). The data of the main peaks are presented in Table 1. The IR peaks of GA at 3400, 2931, 1072 cm^{-1} are assigned to the stretching vibration of –OH, –CH, and the galactose backbone, respectively;[30] those around 1616 and 1417 cm^{-1} are due to asymmetric and symmetric stretching vibrations of carboxyl groups of galacturonic acid units, respectively.[31] Comparing the IR peaks of ZnS

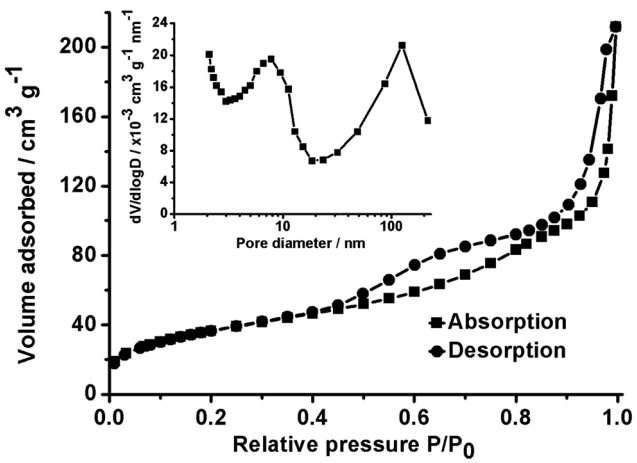

Fig. 2 Nitrogen adsorption–desorption isotherms and pore size distribution plot (inset) of ZnS FPNSs.

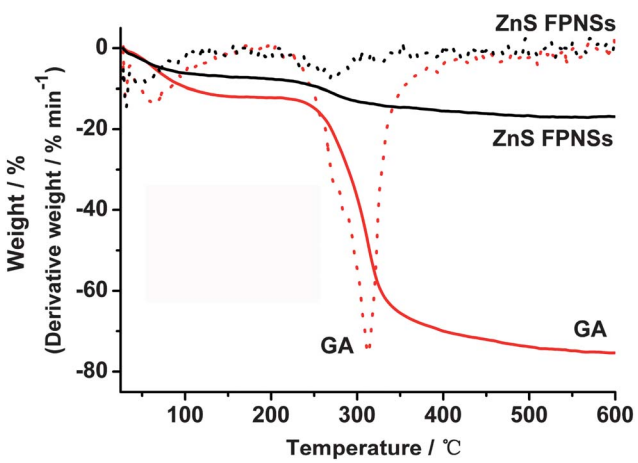

Fig. 3 TGA thermograms (solid line) and the corresponding DTG plots (dashed line) of ZnS FPNSs and GA.

Table 1 The main IR peaks of GA and ZnS FPNSs from their IR spectra

Assignment	–OH/cm^{-1}	–CH/cm^{-1}	$\nu_{as(-COO^-)}$/cm^{-1}	$\nu_{s(-COO^-)}$/cm^{-1}	galactose backbone/cm^{-1}
GA	3400	2931	1616	1417	1072
ZnS FPNSs	3423	2927	1633	1398	1070

FPNSs with those of GA, there are negligible variations in the characteristic peaks of –CH groups and galactose backbone; but the typical peaks of –OH and $–COO^-$ groups have shifted by about 20 cm^{-1}. This evidence not only confirms the existence of GA or its fragments in the nanospheres, but also indicates that there might be coordination interaction between zinc ions and hydroxyl and carboxyl groups of GA, which may play an important role in the formation and improvement of colloidal stability of the porous nanospheres.[32]

On the basis of the above observations and discussion, a plausible mechanism based on the coordination nucleation and Ostwald ripening is proposed to address the formation of ZnS FPNSs. Zn^{2+} firstly coordinated with some groups of GA (such as hydroxyl and carboxyl groups) when mixing, resulting in locally high zinc ion concentrations around these groups. After TAA was added, the slow-released S^{2-} ions reacted with Zn^{2+} ions to form ZnS nuclei on these special sites of GA.[33] When the hydrothermal treatment was carried out, the high concentration of ZnS nuclei will "focus" the size distribution, and numerous nanograins with a diameter of several nanometers were formed.[34] Because GA molecules tend to aggregate through the interaction of the intra- and inter-molecular hydrogen bonds and the crystal growth is isotropic, the formation of a spherical morphology seems to be reasonable through the aggregation of these nuclei and GA to achieve the minimization of their surface energy.[35] Further hydrothermal treatment led to the growth of ZnS nuclei in the Ostwald ripening process, leaving behind the open and accessible porous structures. The formation of ZnS FPNSs could be described as follows:

$$GA + Zn^{2+} \rightarrow GA - Zn^{2+}$$

$$GA - Zn^{2+} + CH_3CSNH_2 \rightarrow GA - ZnS$$

$$GA{-}ZnS \xrightarrow{\text{aggregation}} ZnS \quad FPNSs$$

The above presumption could be verified by prolonging the hydrothermal time to 24 h, in which larger nanocrystals and more space are observed (ESI,† Fig. S3) and elevating the hydrothermal temperature to 140 °C, in which hollow structures of the nanospheres appeared (ESI,† Fig. S4). That is to say, we can also tune the microstructures of the nanospheres by changing the experimental conditions.

Fig. 4 shows the UV–vis absorption and PL spectra of the porous nanospheres. Its UV–vis spectra is a rather featureless curve with gradually increasing absorbance toward shorter wavelengths (Curve A). This phenomenon is likely to be due to the overlap of absorption bands, which occur at different energies for nanocrystals having disparate sizes.[32] The PL spectrum

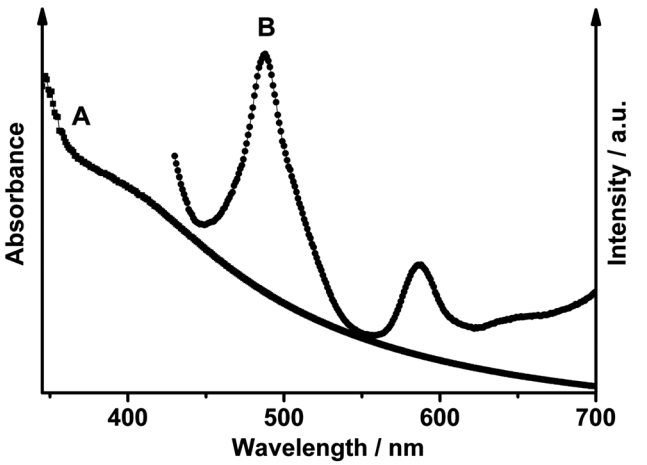

Fig. 4 UV–vis (A) and PL spectra (B) of ZnS FPNSs.

was measured with the excitation wavelength of 400 nm. A relatively narrow and strong emission peak is observed centered at 488 nm, accompanied by a small peak at 588 nm (Curve B). The PL signals presumably resulted from the surface and deep trapped state's emission, respectively.[19,36] The fluorescence intensity of the ZnS FPNSs had negligible change even after one month of storage, indicating its excellent photostability. Even though the quantum yield is relatively low and not comparable to Cd-based quantum dots, ZnS FPNSs exhibit satisfactorily photostable emission signals, which makes them advantageous as a fluorescent tracer for living cell imaging.[37]

Particle size measurements determined by DLS show that ZnS FPNSs possess a mean hydrodynamic diameter of about 92 nm in H_2O (ESI,† Fig. S5). The stability was evaluated by monitoring their zeta potential and hydrodynamic size in the complete cell medium DMEM containing 10% FBS over a four-day period. As shown in Fig. S6,† the zeta potential and hydrodynamic size of ZnS FPNSs didn't show major changes after 96 h, indicating the relatively higher stability of these nanospheres in biological fluids at physiological pH values. This is possibly due to the existence of the highly branched polysaccharide structures of GA, which supply steric repulsion between nanoparticles and improve the colloidal stability.[24] These properties make ZnS FPNSs suitable for being injected intravenously for *in vivo* studies, which would avoid the removal from the blood pool by reticuloendothelial system and find their way through the blood vessels to tumors.[38]

One of the prerequisites for the carrier material serving for biomedical applications is that it should be of low-toxicity.[39] The cytotoxicity of ZnS FPNSs was tested on HeLa cells by an MTT assay, which is regarded as a routine method before further biocompatible studies.[12] As shown in Fig. 5, the viability of

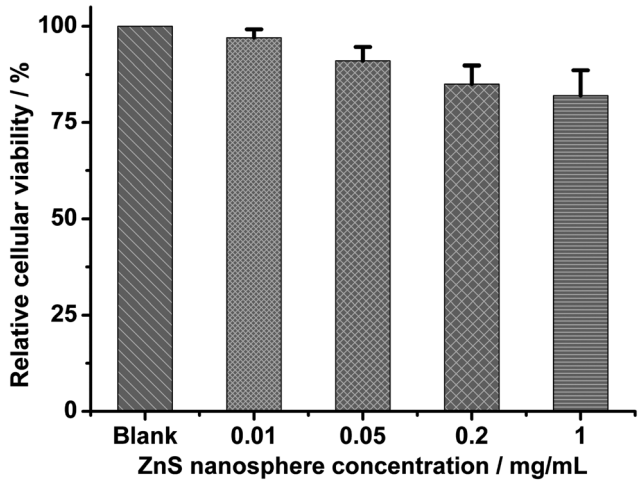

Fig. 5 Cytotoxic profiles of ZnS FPNSs at concentrations of 0.01–1 mg mL^{-1} against HeLa cellls determined by MTT assay after 24 h, with untreated cells as a negative reference.

untreated cells in the blank group was assumed to be 100%; after ZnS FPNSs were incubated with the cells for 24 h, the cellular viability remains above 80% even up to doses of 1 mg mL^{-1}. The preliminary results indicate that these nanospheres barely exhibit toxicity at the cellular level, which means they might be suitable for use inside cells and even *in vivo* applications.[14]

3.2 Application of ZnS FPNSs for potential drug delivery and live cell imaging

To investigate the potential application of ZnS FPNSs as drug carriers, loading and *in vitro* release studies were carried out as follows. The porosity provides molecular accessibility. In this work, ST was loaded as a model drug into the porous nanospheres by post-adsorption and the ST-loaded nanospheres are denoted as the ST–ZnS system. The loading was examined by FTIR (ESI,† Fig. S7) and the measurement of the zeta potential of ZnS FPNSs before and after loading ST. In comparison with the zeta potential of ZnS FPNSs (−20 mV), that of the ST–ZnS system decreased to −13 mV. We speculate that the negatively charged carboxyl groups on ZnS FPNSs might be neutralized by the positively charged ST during the loading process.[17] In addition, the loading ability was estimated to be about 15% by the comparison of the fluorescence intensity of ST solution before and after loading (ESI,† Fig. S8), although the aggregation of the encapsulated ST molecules also might cause a decrease in the fluorescence intensity. This result implies that the nanospheres might have a good adsorption capacity and that the mesopores are open and accessible.

The *in vitro* release kinetics of ST from the ST–ZnS system was studied against PBS buffer at 37 °C (ESI,† Fig. S9). An initial burst release was observed within the first 2 h. Thereafter, ST exhibited a diffusion-controlled release under a mimic physiological condition (pH 7.4) with $t_{1/2} = 6$ h (the time needed for the release of 50% of the dose).[11] The cumulative release reached a value of 82% after 24 h and extended over 50 h.

To further examine whether the ST–ZnS system was uptaken into cells, their colocalization was visualized using CLSM after being incubated with HeLa cells for 6 h. The fluorescence signals of ZnS FPNSs and ST were collected using a dual-channel mode as green dots and red dots, respectively.[40] As shown in Fig. 6, a remarkable intracellular fluorescence was found localized in the cytoplasm and aggregated at the periphery of the nucleus. Part of the red fluorescence coincides with the green fluorescence, giving the orange color after the overlay of the channels, which suggests part of the loaded ST remained inside the porous nanospheres. But as indicated by the arrow in Fig. 6D, a fraction of the loaded ST also escaped from the nanospheres. This evidence visually confirms that the ST–ZnS system could penetrate into living cells and also that the loaded ST could be released from the nanospheres. In this way, the use of ZnS FPNSs as a carrier for potential drug delivery and as a fluorescent tracer for live cell imaging with real-time monitoring properties was demonstrated.

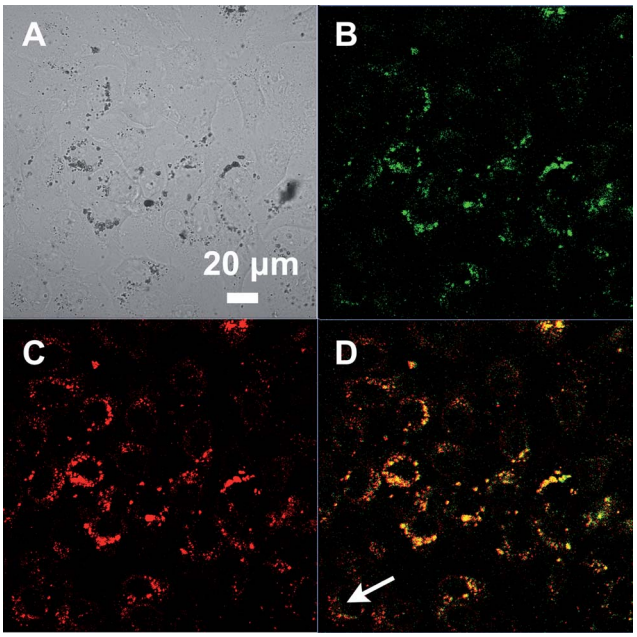

Fig. 6 Confocal fluorescence images of the ST–ZnS system endocytosed by HeLa cells determined by using a dual-channel mode of CLSM. Panel A, the bright-field transmission image; Panel B, green indicates the fluorescence of ZnS FPNSs excited at 405 nm and the emission collected in the range of 460–520 nm; Panel C, red indicates the fluorescence of ST excited at 543 nm and the emission collected in the range of 555–600 nm; Panel D, orange indicates the merged fluorescence of B and C, showing the coincidence of green and red spots.

Conclusions

In summary, ZnS FPNSs were successfully synthesized by a facile GA-assisted hydrothermal approach. They exhibit excellent colloidal stability, photostable fluorescent signals, good biocompatibility, and accessible porous structure. A plausible mechanism based on the coordination nucleation and Ostwald ripening is proposed to address the formation of ZnS FPNSs. Their potential as multifunctional nanoplatforms was demonstrated with ST as a model drug for simultaneous drug delivery and optical imaging by the CLSM observations. Furthermore, the ability to image in this way may be exploited in other biomedical research and nanomedicines. This approach may be

further developed into a promising strategy for targeted delivery when conjugated with specific antibodies and peptides.

Acknowledgements

This work was financially supported by the National Natural Science Foundation of China (21101056, 21105021) and Educational Commission of Henan Province of China (2011A150005). We thank Prof. Zijian Guo for helpful advice, and Dr Changli Zhang and Chengcheng Zhu for CLSM characterization and discussion.

Notes and references

1 T. M. Allen and P. R. Cullis, *Science*, 2004, **303**, 1818.
2 X. Y. Chen, S. S. Gambhir and J. Cheon, *Acc. Chem. Res.*, 2011, **44**, 841.
3 I. I. Slowing, J. L. Vivero-Escoto, C. W. Wu and V. S. Y. Lin, *Adv. Drug Delivery Rev.*, 2008, **60**, 1278.
4 R. M. Xing, X. Y. Wang, C. L. Zhang, Y. M. Zhang, Q. Wang, Z. Yang and Z. J. Guo, *J. Inorg. Biochem.*, 2009, **103**, 1039.
5 R. M. Xing, X. Y. Wang, L. L. Yan, C. L. Zhang, Z. Yang, X. H. Wang and Z. J. Guo, *Dalton Trans.*, 2009, 1710.
6 Y. N. Xia, W. Y. Li, C. M. Cobley, J. Y. Chen, X. H. Xia, Q. Zhang, M. X. Yang, E. C. Cho and P. K. Brown, *Acc. Chem. Res.*, 2011, **44**, 914.
7 B. Luo, S. Xu, A. Luo, W. R. Wang, S. L. Wang, J. Guo, Y. Lin, D. Y. Zhao and C. C. Wang, *ACS Nano*, 2011, **5**, 1428.
8 J. L. Gu, S. S. Su, Y. S. Li, Q. J. He and J. L. Shi, *Chem. Commun.*, 2011, **47**, 2101.
9 J. E. Lee, N. Lee, T. Kim, J. Kim and T. Hyeon, *Acc. Chem. Res.*, 2011, **44**, 893.
10 N. Erathodiyil and J. Y. Ying, *Acc. Chem. Res.*, 2011, **44**, 925.
11 K. Cheng, S. Peng, C. J. Xu and S. H. Sun, *J. Am. Chem. Soc.*, 2009, **131**, 10637.
12 Y. Fang, D. Gu, Y. Zou, Z. X. Wu, F. Y. Li, R. C. Che, Y. H. Deng, B. Tu and D. Y. Zhao, *Angew. Chem., Int. Ed.*, 2010, **49**, 7987.
13 D. L. Shi, Y. Guo, Z. Y. Dong, J. Lian, W. Wang, G. K. Liu, L. M. Wang and R. C. Ewing, *Adv. Mater.*, 2007, **19**, 4033.
14 M. Baker, *Nat. Methods*, 2010, **7**, 957.
15 A. M. Derfus, W. C. W. Chan and S. N. Bhatia, *Nano Lett.*, 2004, **4**, 11.
16 Y. Y. Su, Y. He, H. T. Lu, L. M. Sai, Q. N. Li, W. X. Li, L. H. Wang, P. P. Shen, Q. Huang and C. H. Fan, *Biomaterials*, 2009, **30**, 19.
17 J. H. Park, L. Gu, G. von Maltzahn, E. Ruoslahti, S. N. Bhatia and M. J. Sailor, *Nat. Mater.*, 2009, **8**, 331.
18 F. Chen, Y. J. Zhu, K. H. Zhang, J. Wu, K. W. Wang, Q. L. Tang and X. M. Mo, *Nanoscale Res. Lett.*, 2011, **6**, 1.
19 W. B. Zhou, D. T. Schwartz and F. Baneyx, *J. Am. Chem. Soc.*, 2010, **132**, 4731.
20 D. Zhu, X. X. Jiang, C. Zhao, X. L. Sun, J. R. Zhang and J. J. Zhu, *Chem. Commun.*, 2010, **46**, 5226.
21 Z. X. Wang, L. M. Wu, M. Chen and S. X. Zhou, *J. Am. Chem. Soc.*, 2009, **131**, 11276.
22 L. Gu, J. H. Park, K. H. Duong, E. Ruoslahti and M. J. Sailor, *Small*, 2010, **6**, 2546.
23 Y. M. Guo, J. Zhang, L. Yang, H. J. Wang, F. F. Wang and Z. Zheng, *Chem. Commun.*, 2010, **46**, 3493.
24 V. Kattumuri, K. Katti, S. Bhaskaran, E. J. Boote, S. W. Casteel, G. M. Fent, D. J. Robertson, M. Chandrasekhar, R. Kannan and K. V. Katti, *Small*, 2007, **3**, 333.
25 L. Zhang, F. Q. Yu, A. Cole, B. Chertok, A. David, J. K. Wang and V. Yang, *AAPS J.*, 2009, **11**, 693.
26 L. M. Lang, B. J. Li, W. Liu, L. Jiang, Z. Xu and G. Yin, *Chem. Commun.*, 2010, **46**, 448.
27 J. S. Hu, L. L. Ren, Y. G. Guo, H. P. Liang, A. M. Cao, L. J. Wan and C. L. Bai, *Angew. Chem., Int. Ed.*, 2005, **44**, 1269.
28 M. Vallet-Regi, F. Balas and D. Arcos, *Angew. Chem., Int. Ed.*, 2007, **46**, 7548.
29 M. J. Zohuriaan and F. Shokrolahi, *Polym. Test.*, 2004, **23**, 575.
30 X. L. Zhou, P. N. Sun, P. Bucheli, T. H. Huang and D. F. Wang, *J. Agric. Food Chem.*, 2009, **57**, 5121.
31 E. A. Hugo, S. C. Ofelia, V. T. Humberto, J. V. C. Eduardo and L. C. Consuelo, *Carbohydr. Polym.*, 2010, **79**, 541.
32 L. Yang, R. M. Xing, Q. M. Shen, K. Jiang, F. Ye, J. Y. Wang and Q. S. Ren, *J. Phys. Chem. B*, 2006, **110**, 10534.
33 H. J. Liu, Y. H. Ni, M. Han, Q. Liu, Z. Xu, J. M. Hong and X. M, *Nanotechnology*, 2005, **16**, 2908.
34 X. Peng, L. Manna, W. Yang, J. Wickham, E. Scher, A. Kadavanich and A. P. Alivisatos, *Nature*, 2000, **404**, 59.
35 S. H. Liu, R. M. Xing, F. Lu, R. K. Rana and J. J. Zhu, *J. Phys. Chem. C*, 2009, **113**, 21042.
36 Z. W. Quan, Z. L. Wang, P. P. Yang, J. Lin and J. Y. Fang, *Inorg. Chem.*, 2007, **46**, 1354.
37 E. W. Miller, S. X. Bian and C. J. Chang, *J. Am. Chem. Soc.*, 2007, **129**, 3458.
38 J. Zhu, J. W. Tang, L. Z. Zhao, X. F. Zhou, Y. H. Wang and C. Z. Yu, *Small*, 2010, **6**, 276.
39 R. M. Xing, S. H. Liu and S. F. Tian, *J. Nanopart. Res.*, 2011, **13**, 4847.
40 Z. P. Liu, C. L. Zhang, W. J. He, Z. H. Yang, X. Gao and Z. J. Guo, *Chem. Commun.*, 2010, **46**, 6138.

